World Scientific
www.worldscientific.com

ENERGY HARVESTING IN PIEZOELASTIC SYSTEMS DRIVEN BY RANDOM EXCITATIONS

M. BOROWIEC and G. LITAK[*]

Faculty of Mechanical Engineering
Lublin University of Technology
PL-20-618 Lublin, Poland
[*]g.litak@pollub.pl

M. I. FRISWELL, S. F. ALI, S. ADHIKARI,
A. W. LEES and O. BILGEN

College of Engineering, Swansea University
Singleton Park, Swansea SA2 8PP, UK

The inverted elastic beam is proposed as an energy harvester. The beam has a tip mass and piezoelectric layers which transduce the bending strains induced by the stochastic horizontal displacement into electrical charge. The efficiency of this nonlinear device is analyzed, focusing on the region of stochastic resonance where the beam motion has a large amplitude. Increasing the noise level allows the motion of the beam system to escape from single well oscillations and thus generate more power.

Keywords: Energy harvesting; random excitation; cantilever beam; bistable oscillator.

1. Introduction

Recently, the demands on portable devices, self-powered wireless sensors and similar applications that currently require rechargeable batteries, have increased considerably.[1−4] Vibration energy is one of the candidate technologies, in competition with other possibilities such as photo-voltaic or thermal gradient approaches.[5,6] The effectiveness of devices based on harvesting vibration energy and their availability are continuously growing.[7] Ambient mechanical vibrations can be converted to the electrical energy using electromagnetic, piezoelectric, and electrostatic methods.[1,5,7] Piezoelectric transducers can be easily integrated into elastic multilayer cantilever beams; Priya[8] reviewed potential piezoelectric materials for energy harvesting and discusses various prototypes.

The main advantage of piezoelectric devices, compared to electrostatic and electromagnetic devices, is their high power output for a given device volume and excitation.[6,8] Although not suitable for generating high power levels, they are very suitable for applications to small electronic devices. The main issue with this form of harvester is the source of ambient energy. The classic approach is to tune the mechanical part of the harvester to resonate; this approach is good for narrow band excitations but performs poorly in off-resonance conditions or with broadband ambient excitation.[1,4] Unfortunately, the small levels of energy available off-resonance is often insufficient and a tuning process has to be employed. Ambient excitation forces, such as wind and road traffic motion, often provide changeable conditions characterized by fluctuating frequency and amplitude, or by broadband excitation. Thus, the ideal device is a broadband harvester which is not critically sensitive to the specific frequency or amplitude of excitation.[5,6] One approach is a nonlinear mechanical resonator with a dual well potential, obtained using a magnetic field or special prestressed conditions.[9−12]

Recently, Friswell *et al.*[13] studied a piezoelastic system consisting of a cantilever beam with a tip mass that was mounted vertically and harmonically excited in the transverse direction at its base. For a relatively large tip mass the vertical position was unstable and the beam buckled, giving a double well potential due to gravitational loading. The deterministic model was simulated and validated using an experimental device with three different tip masses, representing three interesting cases: a linear system; a low natural frequency, nonbuckled beam; and a buckled beam. The most practical configuration appeared to be the pre-buckled case, where the proposed system has a low natural frequency, a high level of harvested power, and an increased bandwidth over a linear harvester.

In the present paper, we follow the above mentioned model (Friswell *et al.*[13]) and complete the analysis by simulating an inverted beam excited by random noise. Similar approaches to a broadband piezoelastic device using random noise excitation have been discussed in Refs. 11, 14−20. Note also that the nonlinear system considered in this paper bends due to the gravitational field (Fig. 1), in contrast to the magnetic systems discussed in previous papers.[11,14−20] More recent analysis on nonlinear beam system vibrations can be found in Refs. 21, 22, 23.

2. Equations of Motion

Figure 1 shows a schematic of the system considered, which consists of an inverted beam with one end fixed to the moving base and other loaded by a tip mass, m_t. The equation of motion has been derived using Lagrange's method. An arbitrary point at the beam denoted by mass element dm at distance x from the oscillating base and the point mass m_t were considered, which undergo a flexible body deflection to a new position due to the base excitation. The mass element of the beam dm undergoes a horizontal displacement $y + v_{dm}$ and a vertical displacement $(-u_{dm})$ and a rotation
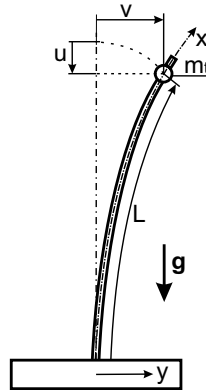
Fig. 1. The model of the inverted beam with a tip mass m_t with its horizontal and vertical displacements v and u. L is the length of beam, while x is the axis oriented along the beam. **g** represents the gravitational acceleration while, y denotes the kinematic horizontal excitation.

of ϕ of the tip beam point (Fig. 1). Note that in our calculations, the effect of rotary inertia of the beam mass, ϕ_{dm}, was neglected.

The kinetic energy of the system is[13,24,25]

$$T = \frac{1}{2}\rho A \int_m [(\dot{v}_{dm}(x,t) + \dot{y}(t))^2 + \dot{u}_{dm}(x,t)^2]\mathrm{d}x$$
$$+ \frac{1}{2}m_t[(\dot{v}(t) + \dot{y}(t))^2 + \dot{u}(t)^2] + \frac{1}{2}I_0\dot{\phi}^2 \tag{1}$$

and the potential energy arising from the strain in the elastic beam, and gravity terms from the beam and tip mass, is

$$\Pi = \frac{1}{2}EI \int_0^L \kappa(x,t)^2\mathrm{d}x + g\rho A \int_m u_{dm}(x,t)\mathrm{d}x + m_t g u(t). \tag{2}$$

A single degree of freedom model of the deflection of the beam is considered, where

$$v_{dm}(x,t) = v(t)\psi(x) \tag{3}$$

for some known function $\psi(x)$ that approximates the deformation in the beam. By neglecting terms higher than third order the horizontal deflection of the beam u_{dm} may be written in terms of the primary degree of freedom v. Thus, the kinetic and potential energies may be written in terms of v and Lagrange's method applied to derive the equation of motion of the beam-mass system[13]

$$[m_t + \rho A N_1 + I_0 N_5^2 + (\rho A N_3 + m_t N_4^2 + I_0 N_5^4)v^2]\ddot{v} + [\rho A N_3 + m_t N_4^2 + I_0 N_5^4]v\dot{v}^2$$
$$- [g(m_t N_4 + \rho A N_9) - EI(N_6 + 2N_7 v^2)]v = -[m_t + \rho A N_2]\ddot{y}, \tag{4}$$

where $\ddot{y}$ is the acceleration of the base of the beam and is assumed to be stochastic and of the form

$$\ddot{y} = \Gamma(t), \tag{5}$$

Table 1. System parameters.

Symbol and value	Description
$L = 0.2\,\text{m}$	Length of the beam
$m_t = 0.038\,\text{kg}$	Tip mass
$\rho = 7850\,\text{kg/m}^3$	Density of the beam mass
$A = 0.000004\,\text{m}^2$	Cross-section area of beam
$E = 210\,\text{GPa}$	Young's modulus
$I = 2.15 \times 10^{-14}\,\text{m}^4$	Geometrical moment of inertia
$I_0 = 1144.4 \times 10^{-3}\,\text{kgm}^2$	Mass moment of inertia
y	Kinematic displacement of the base
$C_p = 38.9\,\text{nF}$	Capacitance of the piezoelectric patches
$R = 50\,\text{k}\Omega$	Load resistance
$L_p = 28\,\text{mm}$	Active length of piezoelectric layers
$b_b = 15\,\text{mm}$	Beam width
$h_b = 2.5\,\text{mm}$	Beam thickness
$h_p = 300\,\mu\text{m}$	Piezoelectric layers thickness
$e_{31} = -5.157\,\text{C/m}^2$	Piezoelectric constant

Table 2. Effective parameters in SI units [see Eqs. (4)−(7)]; the corresponding definitions can be found in Appendix.

N_1	N_2	N_3	N_4	N_5	N_6	N_7	N_8	N_9
0.0453521	0.072676	1.3801	6.1685	7.85398	380.504	5867.85	180979.	0.36685

where $\Gamma(t)$ denotes the stochastic factor. The other parameters used are defined in Tables 1 and 2.

3. The Coupled Piezoelectric Model

Using the derivation of the coupled electro-mechanical model provided by the authors,[13] the equation of motion combined with the electrical equation becomes

$$
\begin{aligned}
&[m_t + \rho A N_1 + I_0 N_5^2 + (\rho A N_3 + m_t N_4^2 + I_0 N_5^4)v^2]\ddot{v} \\
&+ [\rho A N_3 + m_t N_4^2 + I_0 N_5^4]v\dot{v}^2 \\
&\quad - [g(m_t N_4 + \rho A N_9) - EI(N_6 + 2N_7 v^2)]v - DU = -[m_t + \rho A N_2]\ddot{y} \\
&C_p \dot{U} + \frac{U}{R} + D\dot{v} = 0,
\end{aligned}
\tag{6}
$$

where U is the voltage across the load resistor connected to the piezoelectric patch, C_p is the capacitance of the piezoelectric patches and R is the load resistance. Two piezoelectric patches are attached to the beam and connected in parallel. The constant for the electromechanical coupling is given by

$$
D = e_{31} b_p (h_p + h_b) \int_0^{L_p} \psi''(x)\mathrm{d}x = e_{31} b_p (h_p + h_b)\psi'(L_p),
\tag{7}
$$

where h_b is the beam thickness, h_p is the piezoelectric layer thickness, b_p is the piezoelectric layer width, L_p denotes active length of piezoelectric layer, and e_{31} is the piezoelectric constant.

4. Numerical Results and Discussion

Based on Eq. (6), numerical simulations of the beam system with attached piezo-electric layers (Fig. 1) have been performed. We assumed a kinematic excitation, where $\ddot{y}$ was expressed as the random noise factor $\Gamma(t)$ [Eq. (5)]. In the simulations two different kinds of noise were used; Gaussian noise with a normal distribution (ND), and noise with a uniform distribution (UD). The results of the simulations are presented in Figs. 2(a)−2(d).

Figure 2(a) shows the displacement signal to noise ratio σ_v/σ_F (in terms of the corresponding standard deviations) versus the input noise represented by σ_F for a tip mass of $m_t = 0.038\,\text{kg}$. For both noise distributions [normal (ND) and uniform (UD)] one can observe a clear maximum around $\sigma_v/\sigma_F = 0.25$. This maximum corresponds to a stochastic resonance,[26] which gives the largest amplitude oscillation for a given excitation level, and reflects the transition in the system response from single potential well oscillations to double well vibration characteristics with hopping between the two potential wells. One can note that for the normal noise excitation the transition happens for a smaller noise intensity, σ_F, and this because of the long tails of the Gaussian white noise distribution. Such a tail can generate much larger
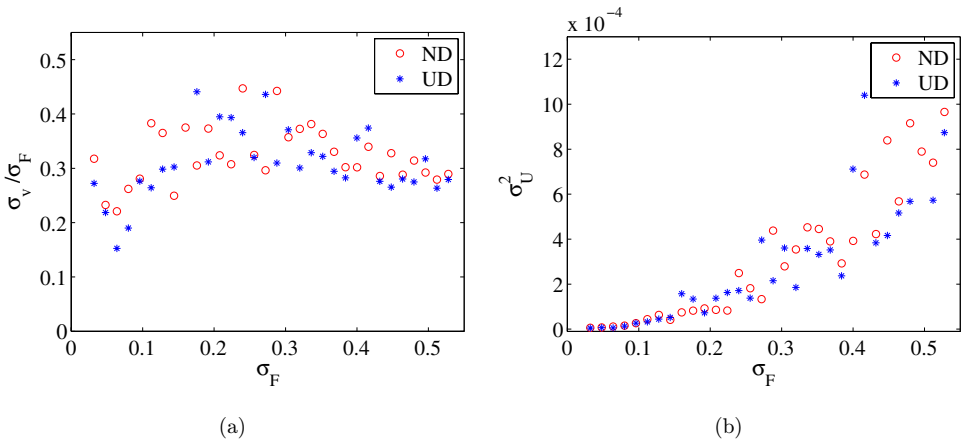

(a)   (b)

Fig. 2. The displacement signal to noise ratio σ_v/σ_F versus σ_F for tip mass $m_t = 0.038\,\text{kg}$ (a), the variance of the generated voltage U for the corresponding tip mass m_t (b), the number of hops (c) and the mean of displacement (d). Two different kinds of noise have been used: normal (ND) and uniform distributions (UD). The simulation time period was fixed as $t \in [0, 10800\,\text{s}]$, while the time step was $\delta t = 0.01\,\text{s}$. The initial time interval for each simulation $[0, 7200\,\text{s}]$ was neglected as a transient in the statistical estimation of the standard deviation σ_F, the number of hops and mean value of displacement $\langle v \rangle$. The initial conditions for each noise level were $[v, \dot{v}, U]_{|t=0} = [0.1042\,\text{m}, 0, 0]$. Each point on the figures is an average of ten different noise realizations.
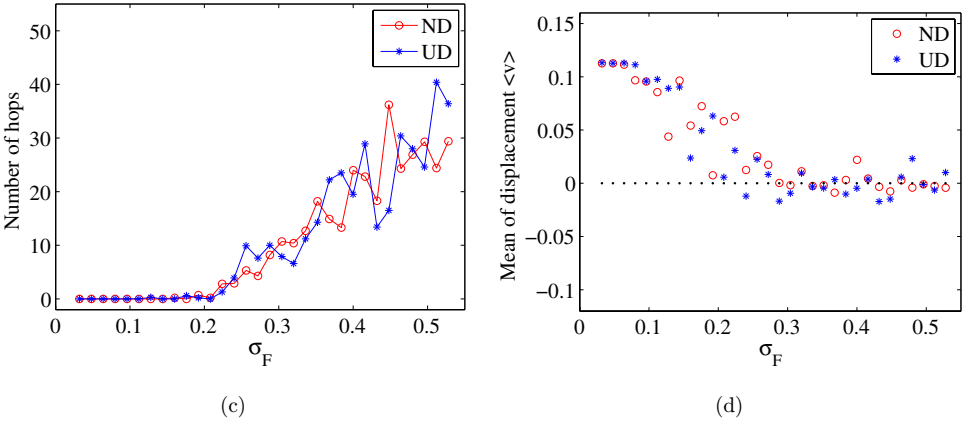
(c)

(d)

Fig. 2. (*Continued*)

accelerations than for the bounded uniform noise case. Consequently, in the region of fairly small σ_v, the value of σ_v/σ_F is slightly larger for ND than for UD. The variance of the voltage output, U [Fig. 2(b)], increases considerably after σ_F passes the stochastic resonance case.

Additionally, we plotted the number of hops between the potential wells [Fig. 2(c)]. As mentioned earlier these are strictly connected to the appearance of the stochastic resonance. Note that the appearance of a larger number of hops in Fig. 2(c) coincidences with the maxima in Fig. 2(a). The effect of this solution bifurcation from single to double well oscillations is also visible in the estimated mean value of displacement $\langle v \rangle$ [Fig. 2(d)]. A displacement mean of $\langle v \rangle \approx 0.11\,\text{m}$ means that the solution oscillates around the beam equilibrium $v_0 \approx 0.1042\,\text{m}$, where v_0 can be
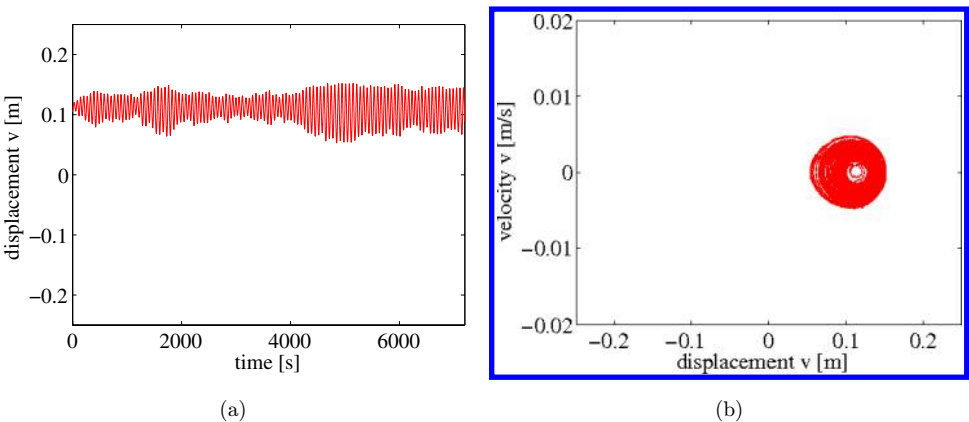

(a)

(b)

Fig. 3. Simulation results for $\sigma_F = 0.200\,\text{N}$ and tip mass $m_t = 0.038\,\text{kg}$, with Gaussian white noise (ND) excitation $\Gamma(t)$: displacement time series (a), phase portrait (b), voltage time series (c), hops from the time simulation (d). Note that the number of hops is 0 as the solution is localized around the buckled beam equilibrium v_0.
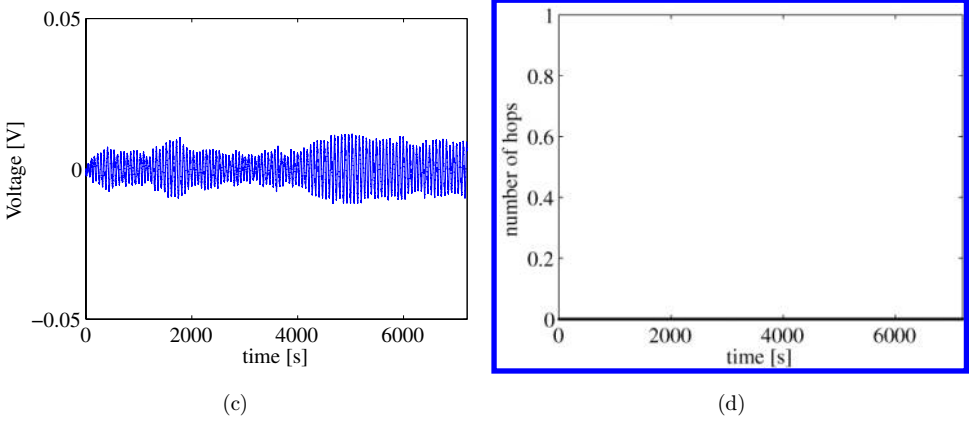
(c)

(d)

Fig. 3.   (*Continued*)

found from the minimum of the potential energy [Eq. (2)] as

$$v_0 = \sqrt{\frac{g(m_t N_4 + \rho A N_9) - IE N_6}{2 E I N_7}}, \tag{8}$$

while any other value corresponds to cases with hopping (for $\sigma_v > 0.25$). The positive $\langle v \rangle$ mimics the asymmetry in the time series with respect to the horizontal reflection through $v = 0$. This asymmetry is related to the limits of the simulation time, $t \in [0 : 3600]$, and the assumed initial conditions, $v_0 > 0$.

To illustrate the system dynamics, examples of displacement and voltage time series, displacement−velocity phase portraits, and the number of hops between
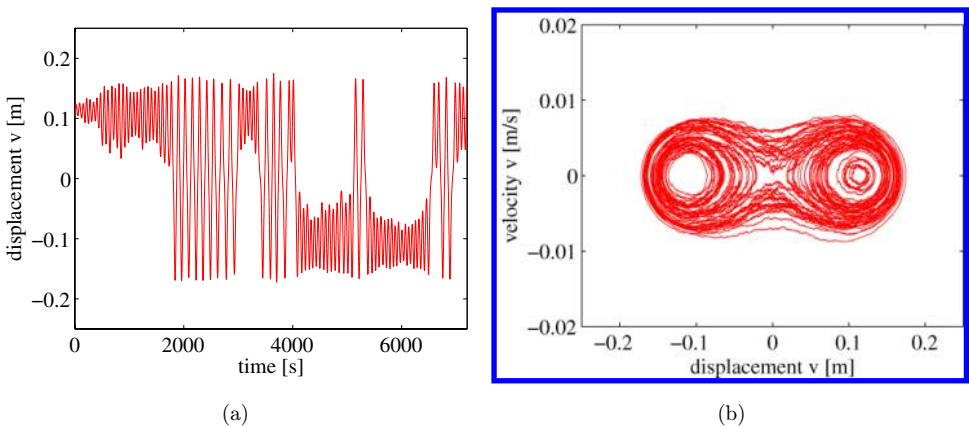

(a)

(b)

Fig. 4. Simulation results for $\sigma_F = 0.320\,\mathrm{N}$ and tip mass $m_t = 0.038\,\mathrm{kg}$, with Gaussian white noise (ND) excitation $\Gamma(t)$: displacement time series (a), phase portrait (b), voltage time series (c) obtained through the single noise realization. Figure 4(d) presents the number of hops between the potential wells. Note that for smaller σ_F [Fig. 3(d)] the number of hops was 0.
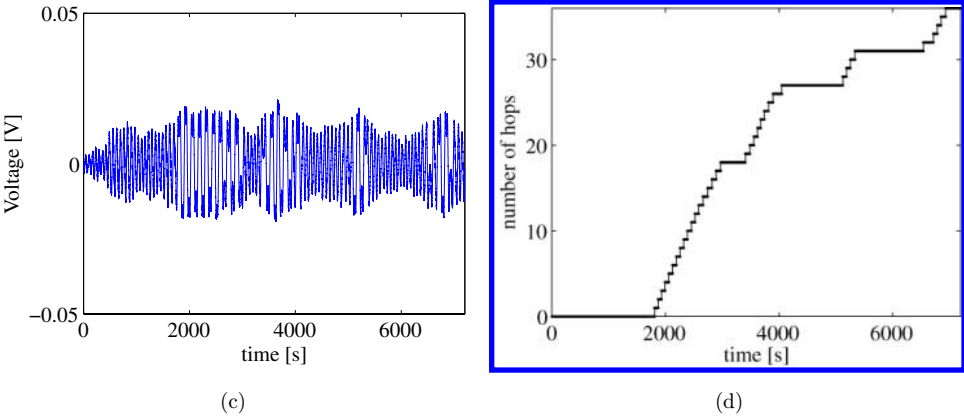
(c)

(d)

Fig. 4.   (*Continued*)

potential wells, were plotted for the solutions with selected noise levels (for the case of ND) in Figs. 3–5. In Fig. 3, $\sigma_F = 0.200\,\text{N}$ and the solution was reduced to a single potential well oscillation [Fig. 3(a)–3(b)]. In contrast, Figs. 4(a)–4(b) (for $\sigma_F = 0.320\,\text{N}$) and Figs. 5(a)–5(b) (for $\sigma_F = 0.528\,\text{N}$) clearly show the double well oscillations with a fairly large amplitude. The corresponding simulation time ($t \in [0, 7200\,\text{s}]$ was longer than that used for the results presented in Fig. 2. The associated number of system hops is illustrated in Figs. 4(d) and 5(d). Note that the hops are intermittent for intermediate values of the excitation noise level $\sigma_F = 0.320\,\text{N}$ [Fig. 4(d)]. In the case of the stronger noise excitation $\sigma_F = 0.528\,\text{N}$ [Fig. 5(d)] the hops appear to be fairly regular. As concluded from Fig. 2(b), the output power strongly increases after passing $\sigma_F = 0.25$. This is also illustrated by the increasing voltage output in Figs. 3(c), 4(c) and 5(c), where the corresponding $U(t)$ time series
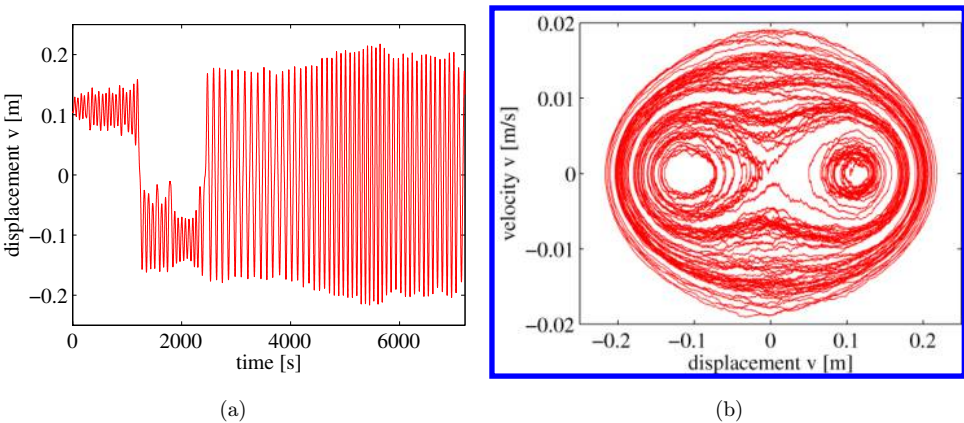

(a)

(b)

Fig. 5. Simulation results for $\sigma_F = 0.528\,\text{N}$ and tip mass $m_t = 0.038\,\text{kg}$, with Gaussian white (ND) noise excitation $\Gamma(t)$: displacement time series (a), phase portrait (b), voltage time series (c), hops from the time simulation (d).
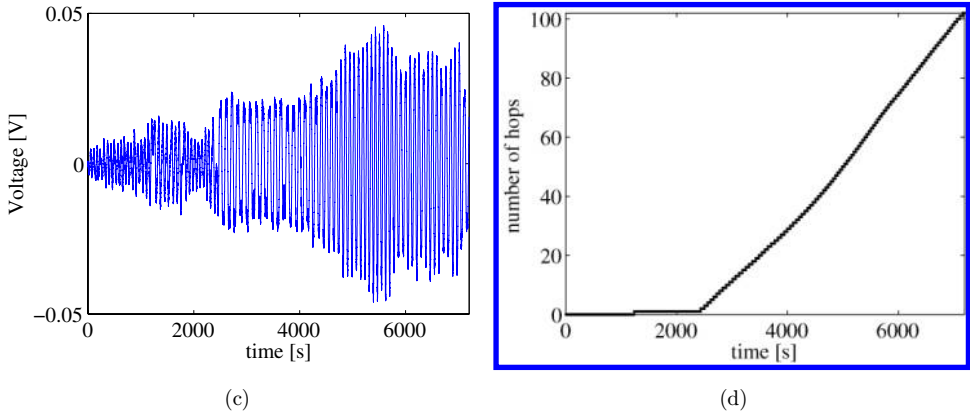
(c)

(d)

Fig. 5. (*Continued*)

are plotted for $\sigma_F = 0.200\,\mathrm{N}$, $0.320\,\mathrm{N}$ and $0.528\,\mathrm{N}$, respectively. These results show an increase in the voltage output.

5. Conclusion

We have analyzed the piezoelectric harvester based on the elastic inverted beam mechanical resonator. Applying the stochastic kinematic excitation to the base we analyzed the voltage output. By increasing the noise level we reported the appearance of the stochastic resonance phenomenon. The simulated results are characterized by relatively large variability [(Fig. 2(a)]. As the results are averaged over ten different noise realizations, this variability occurs in spite of a single set of initial conditions used in all simulations and shows the existence of multiple attractors in the examined system.[13]

As expected from previous studies,[18] the effects of both kinds of noise (ND and UD) are very similar.

It should be noted that for realistic situations the parameters of the mechanical resonator (for instance the tip mass value m_t) can be adjusted to ensure the system is operating in the vicinity of stochastic resonance. In that case the displacement signal to ambient noise ratio has the highest value and the whole system is characterized by the optimum performance. Our experiments on the system with stochastic excitation are in progress and the results will be reported soon.

Appendix

To build the equations of motion [Eq. (4)] we have to evaluate a number of integrals in Eqs. (1) and (2). These can be easily calculated following Ref. 13 and also Refs. 24 and 25, where the deflection model is assumed to be

$$\psi(x) = 1 - \cos\left(\frac{\pi x}{2L}\right).$$

After substituting the above expression into Eqs. (1) to (3), and some lengthly mathematical manipulations,[13,24,25] we obtain the constants N_1 to N_9 (see [Eq. (4)]) as

$$N_1 = \int_0^L \psi(x)^2 \mathrm{d}x = L\left(\frac{3}{2} - \frac{4}{\pi}\right),$$

$$N_2 = \int_0^L \psi(x)\mathrm{d}x = \frac{L}{\pi}(\pi - 2),$$

$$N_3 = \int_0^L \left(\int_0^x \psi'(x)^2 \mathrm{d}x\right)^2 \mathrm{d}x = \frac{\pi^2}{384L}(2\pi^2 - 9),$$

$$N_4 = \int_0^L \psi'(x)^2 \mathrm{d}x = \frac{\pi^2}{8L},$$

$$N_5 = \psi'(L) = \frac{\pi}{2L},$$

$$N_6 = \int_0^L \psi''(x)^2 \mathrm{d}x = \frac{\pi^4}{32L^3},$$

$$N_7 = \int_0^L \psi''(x)^2 \psi'(x)^2 \mathrm{d}x = \frac{\pi^6}{512L^5},$$

$$N_8 = \int_0^L \psi''(x)^2 \psi'(x)^4 \mathrm{d}x = \frac{\pi^8}{4096L^7},$$

$$N_9 = \int_0^L \left(\int_0^x \psi'(x)^2 \mathrm{d}x\right)\mathrm{d}x = \frac{1}{16}(\pi^2 - 4),$$

where $\psi'(x)$ is the derivative $\mathrm{d}\psi(x)/\mathrm{d}x$.

References

1. C. B. Williams and R. B. Yates, Analysis of a micro-electric generator for microsystems, *Sens. Actuators A* **52** (1996) 8−11.
2. S. Roundy, P. Wright and J. Rabaey, *Energy Scavenging for Wireless Sensor Networks*, (Kluwer Academics, Boston, MA, 2003).
3. S. R. Anton, A. Erturk and D. J. Inman, Multifunctional self-charging structures using piesoceramics and thin-film batteries, *Smart Mater. Struct.* **19** (2010) 115021.
4. H. S. Kim, J.-H. Kim and J. Kim, A review of piezoelectric energy harvesting based on vibrations, *Int. J. Prec. Eng. Manuf.* **12** (2011) 1129−1141.
5. L. Tang, Y. Yang and C. K. Soh, Toward broadband vibration-based energy harvesting, *J. Intell. Mater. Syst. Struct.* **21** (2010) 1867−1897.
6. A. Erturk and D. Inman, *Piezoelectric Energy Harvesting* (John Wiley & Sons Ltd., Chichester, UK, 2011).

7. P. D. Mitcheson, E. M. Yeatman, G. K. Rao, A. S. Holmes and T. C. Green, Energy harvesting from human and machine motion for wireless electronic devices, *Proc. IEEE* **96** (2008) 1457−1486.

8. S. Priya, Advances in energy harvesting using low profile piezoelectric transducers, *J. Electroceram.* **19** (2007) 167−184.

9. A. Erturk, J. Hoffmann and D. J. Inman, A piezomagnetoelastic structure for broadband vibration energy harvesting, *Appl. Phys. Lett.* **94** (2009) 254102.

10. E. S. Leland and P. K. Wright, Resonance tuning of piezoelectric vibrations energy scavenging generators using compressive axial preload, *Smart Mater. Struct.* **15** (2006) 1413−1420.

11. G. Litak, M. I. Friswell and S. Adhikari, Magnetopiezoelastic energy harvesting driven by random excitations, *Appl. Phys. Lett.* **96** (2010) 214103.

12. C. A. K. Kwuimy, G. Litak, M. Borowiec and C. Nataraj, Performance of a piezoelectric energy harvester driven by air flow, *Appl. Phys. Lett.* **100** (2012) 024103.

13. M. I. Friswell, S. F. Ali, S. Adhikari, A. W. Lees, O. Bilgen and G. Litak, Nonlinear piezoelectric vibration energy harvesting from a vertical cantilever beam with tip mass, *J. Int. Mat. Syst. Struc.* **23** (2012) 1505−1521.

14. F. Cottone, H. Vocca and L. Gammaitoni, Nonlinear energy harvesting, *Phys. Rev. Lett.* **102** (2009) 080601.

15. E. Halvorsen, Energy harvesters driven by broadband random vibrations, *J. Micromech. Syst.* **17** (2008) 1061−1071.

16. L.-C. J. Blystad and E. Halvorsen, An energy harvester driven by colored noise, *Smart Mater. Struct.* **20** (2011) 025011.

17. M. Ferrari, M. Bau, M. Guizzetti and V. Ferrari, A single-magnet nonlinear piezoelectric converter for enhanced energy harvesting from random vibrations, *Sens. Actuators A Phys.* **172** (2011) 287−292.

18. G. Litak, M. Borowiec, M. I. Friswell and S. Adhikari, Energy harvesting in a magnetopiezoelastic system driven by random excitation with uniform and Gaussian distributions, *J. Theor. Appl. Mech.* **49** (2011) 757−764.

19. N. A. Khovanova and I. A. Khovanov, The role of excitations statistic and nonlinearity in energy harvesting from random impulsive excitations, *App. Phys. Lett.* **99** (2011) 144101.

20. M. F. Daqaq, Transduction of a bistable inductive generator driven by white and exponentially correlated Gaussian noise, *J. Sound Vibr.* **330** (2011) 2554−2564.

21. J. Awrejcewicz and V. A. Krysko, On the vibration of the Euler-Bernoulli beam with clamped ends deflection constraints, *Int. J. Bifur. Chaos* **15** (2005) 1867−1878.

22. I. V. Andrianov and J. Awrejcewicz, On the improved Kirchhoff equation modelling nonlinear vibrations of beams, *Acta Meccanica* **186** (2006) 135−139.

23. J. J. Awrejcewicz, A. V. Krysko, V. Soldatov and V. A. Krysko, Analysis of the nonlinear dynamics of the Timoshenko flexible beams using wavelets, *J. Comput. Nonlinear Dyn.* **7** (2012) 011005.

24. L. D. Zavodney and A. H. Nayfeh, The nonlinear response of a slender bean carrying lumped mass to a principal parametric excitation: Theory and experiment, *Int. J. Non-Linear Mech.* **24** (1989) 105−125.

25. E. Esmailzadeh and G. Nakhaie-Jazar, Periodic behavior of a cantilever beam with end mass subjected to harmonic base excitation, *Int. J. Non-linear Mech.* **33** (1998) 567−577.

26. L. Gammaitoni, P. Hanggi, P. Jung and F. Marchesoni, Stochastic resonance, *Rev. Mod. Phys.* **70** (1998) 223−287.